Supporting Information

Crystalline silicon white light sources driven by optical resonances

Jin Xiang,† Mincheng Panmai,† Shuwen Bai,† Yuhao Ren,‡ Guang-Can Li,† Shulei Li,† Jin Liu,‡ Juntao Li,∗,‡ Miaoxuan Zeng,¶ Juncong She,¶ Yi Xu,§ and Sheng Lan∗,†

†Guangdong Provincial Key Laboratory of Nanophotonic Functional Materials and Devices, School of Information and Optoelectronic Science and Engineering, South China Normal University, Guangzhou 510006, People's Republic of China

‡State Key Laboratory of Optoelectronic Materials and Technologies, School of Physics, Sun Yat-sen University, Guangzhou 510275, People's Republic of China

¶State Key Laboratory of Optoelectronic Materials and Technologies, Guangdong Province Key Laboratory of Display Material and Technology, School of Electronics and Information Technology, Sun Yat-sen University, Guangzhou 510275, People's Republic of China

§and Department of Electronic Engineering, College of Information Science and Technology, Jinan University, People's Republic of China

E-mail: lijt3@mail.sysu.edu.cn; slan@scnu.edu.cn

Table of contents

Supplementary Note 1: Temperature rise in Si nanoparticles induced by femtosecond laser pulses

The temperature of a Si nanoparticle resonantly excited at the magnetic dipole (MD) resonance can be simply estimated by using the carrier density (N) generated in the Si nanoparticle. Assuming 800-nm femtosecond laser light is used to excite the Si nanoparticle and three-photon-induced absorption (3PA) is dominant in the generation of carriers, the total number of photons absorbed by the Si nanoparticles is $3NV$, corresponding to a total energy of $E_p = 3NV \cdot h\nu$. Here, $V = 4\pi R^3/3 \sim 4.0 \times 10^{-21}$ m^3 is the volume of the Si nanoparticle and $h\nu \sim 1.50$ eV $= 2.4 \times 10^{-19}$ J is the energy of a single photon at 800 nm. The radius of the Si nanoparticle with its MD resonance at 800 nm is estimated to be $R \sim 100$ nm. Therefore, the thermal energy generated by the absorbed photons is $Q = (1-\eta) * E_p \sim 2.88 \times 10^{-18}$ J, where $\eta \sim 1.0\%$ is the quantum efficiency of the luminescence (see Ref. 23). On the other hand, the temperature rise in the Si nanoparticle can be calculated by $\Delta T = Q/CM$, where $C = 0.7$ J/(gK) and $M = \rho V = 9.32 \times 10^{-21}$ g are the capacity and mass of the Si nanoparticle. For $N = 10^{21}$ cm^{-3}, the temperature rise in the Si nanoparticle is estimated to be $\Delta T = 441$ K. It implies that the temperature of the Si nanoparticle will reach ~1500 K for a carrier density of $N \sim 3 \times 10^{21}$ cm^{-3}, which can be achieved by exploiting the optical resonances of the Si nanoparticle.

In practice, the Si nanoparticle is excited by femtosecond laser pulses with a repetition rate of 76 MHz. In this case, a steady temperature can be achieved for the Si nanoparticle after absorbing a certain number of laser pulses and it depends strongly on the laser fluence (see Ref. 24). The steady temperature is higher than that induced by a single laser pulse.

Supplementary Note 2: Modification of quantum efficiency by injected carriers

In Figure S1, we present the radiative and nonradiative lifetimes (τ_r and τ_{nr}) as a function of the carrier density in the high injection case. In this case, it is assumed that τ_r is inversely proportional to the injected carrier density (Δn) while τ_{nr} is proportional to the cubic of Δn. The dependence of the quantum efficiency on the carrier density is also provided. It can be seen that the quantum efficiency (η) can be enhanced by nearly four orders of magnitude if the carrier density is increased by one order of magnitude (e.g., from 10^{19} to 10^{20} cm^{-3}). However, it is noticed that the luminescence lifetime is still governed by the nonradiative lifetime (τ_{nr}) although a reduction of the radiative lifetime (τ_r) is observed at high carrier densities. In this case, the reduction of τ_{nr} with increasing temperature is not taken into account. Although the enhancement in η is overestimated, a significant improvement of η is predicted in the high injection case.

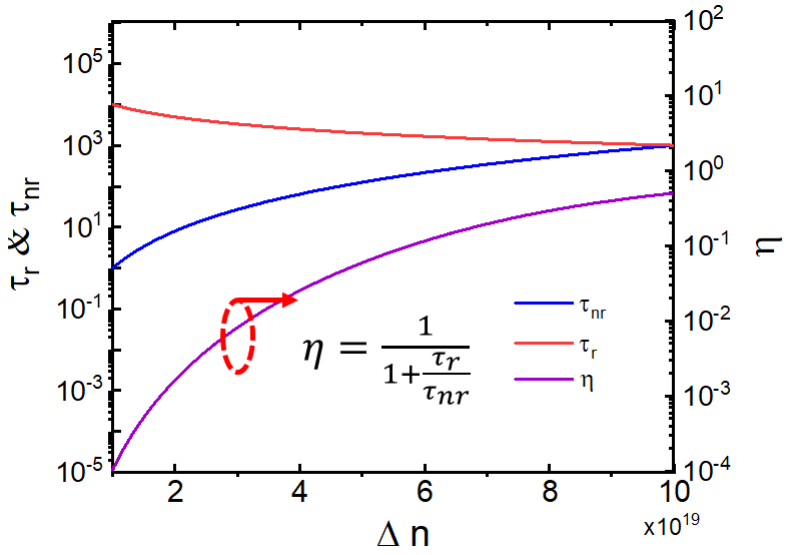

Figure S1 Dependences of the radiative and nonradiative lifetimes on the carrier density in the high injection case. The evolution of the quantum efficiency with increasing carrier density is also provided.

Supplementary Note 3: Carrier densities generated in Si particles with different diameters

It has been confirmed that the carrier dynamics in Si can be modified by injecting dense electron-hole plasma. A large carrier density injected into Si particles is highly desirable for enhancing the quantum efficiency of the hot electron luminescence. When femtosecond laser pulses are employed as the excitation source for Si particles, hot electrons are generated mainly via the two- and three-photon-induced absorption processes (2PA and 3PA). It has been shown that the 2PA and 3PA can be characterized by the integration of $|E|^4$ and $|E|^6$ over the volume of the Si particle. However, the carrier density is inversely proportional to the volume of the Si particle. For example, the creation of only an electron-hole pair in a Si quantum dot with a diameter of 2 nm can lead to a carrier density larger than 1.0×10^{21} cm^{-3} because of the extremely small volume. Therefore, one can use the integration of $|E|^4$ over the volume of the Si particle divided by its volume to characterize the carrier density created in the Si particle. In Figure S2, we compare the relative carrier densities generated in Si particles with diameters (d) of 18, 180 and 1800 nm by using femtosecond laser pulses at 720 nm. It can be seen that the largest carrier density is achieved in Si nanoparticle with d = 180 due to the existence of the magnetic dipole (MD) resonance, which significantly enhance the 2PA of the Si nanoparticle. For the Si quantum dot with d = 18 nm, there is no resonance in the visible to near infrared spectral range and the 2PA is quite small. Although the Si microparticle with d = 1800 nm may support whisper galley modes with large quality factors, their linewidths are much narrower than that of the femtosecond laser pulses. As a result, the generated carrier density in the Si nanoparticle is larger than that in the Si microparticle by a factor of ~50.

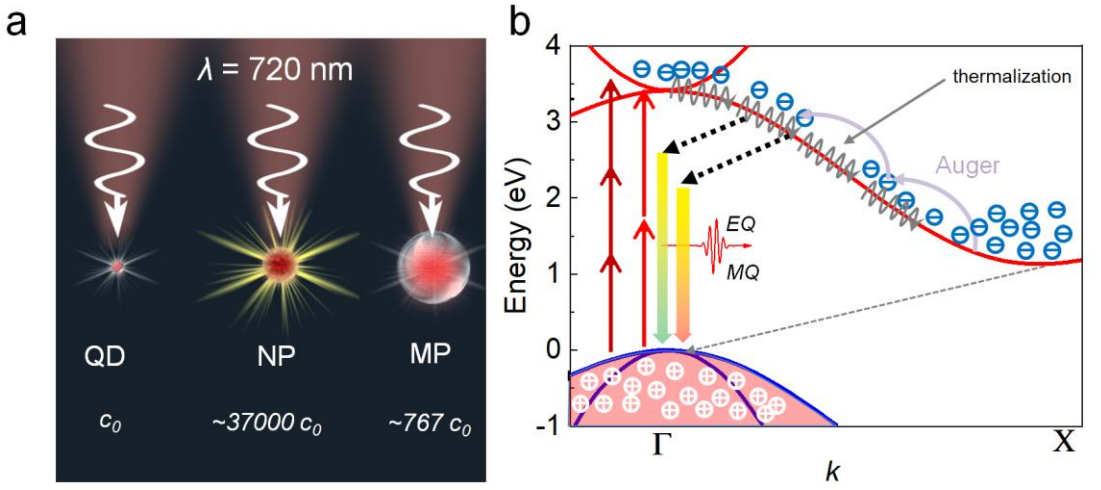

C

d	$V = 4\pi R^3/3$	$E^4 = \int E^4 \, dr$	E^4/V
d = 18 nm	3.05×10^{-24}	1.32×10^{-27}	4.30×10^{-4}
d = 180 nm	3.05×10^{-21}	4.70×10^{-20}	16.00
d = 1800 nm	3.05×10^{-18}	0.95×10^{-18}	0.33

Figure S2 (a) Schematic showing the excitation of three Si particles with different diameters (d = 18, 180, and 1800 nm) by using femtosecond laser pulses. The carrier densities estimated for the Si particles are also provided. (b) Schematic showing the generation of hot electrons in the conduction band of Si via 2PA and 3PA processes. (c) Comparison of the volume and the integration of $|E|^4$ calculated for the three Si particles which are used to derive the values of 2PA.

Supplementary Note 4: Estimation of the temperature in a Si nanoparticle

We proposed in this work a new mechanism to boost the hot electron limunescence by exploiting the intrinsic excitation of carriers from the valence band to the conduction band (Δ point) at a high temperature, as schematically shown in Figure 1a,b. Therefore, it is important to know the temperature of a Si nanoparticle when the luminescence burst occurs above the threshold. So far, it reamins a big challenge to measure the temperature of a nanoparticle from the technical point of view. Therefore, we tried to estimate the temperatue of a Si nanoparticle from its luminescence spectrum.

As discussed in detail in our previous study (see Ref. 24), the Mie resonances supported by a Si nanoparticle will be modified dramatically by injecting dense electron-hole plasma. At high carrier densities, a blue shift of peak wavelength as well as a broadening of linewidth is expected for the Mie resonances due to the change induced in the complex refractive index of Si. On the other hand, a red shift of the Mie resonances is anticipated because of the temperature rise in the Si nanoparticle owing to the thermo-optical effect. Previously, we observed a net blue shift of ~50 nm for the MD resonance at a carrier density of ~10^{20} cm^{-3} (see Figure 3, Ref. 24). As can be seen in Figure 2a, the enhanced luminescence appears exactly at the MQ resonance of the Si nanoparticle, which was measured at room temperature (see also Figure S3a). This behavior implies that the blue shift of the MQ resonance induced by injected carriers is completely counteracted by the red shift induced by the thermos-optical

effect.

In Supplementary Note 1, we have presented a rough estimation of the temperature rise in a Si nanoparticle induced by femtosecond laser pulses at a carrier density of ~3.0 × 10^{21} cm^{-3}. Now we tried to derive the temperature of the Si nanoparticle described above from its luminescence spectra shown in Figure 2a. In Figure S3a, we present the luminescence spectrum of the Si nanoparticle measured at a pulse energy of 10.0 pJ, which is above the threshold for the luminescence burst. As mentioned above, the enhanced luminescence appears exactly at the MQ resonance of the Si nanoparticle, implying the blueshift induced by the injected carriers is counteracted by the reshift induced by the temperature rise. In Figure S3b, we present the dependence of the bandgap energy and refractive index change on temperature calculated for Si due to the thermo-optical effect. In Figure S3c,d, we show the changes in the real (n) and imaginary (κ) parts of the complex refractive index of Si induced by injected carriers of different densities. From Figure S3a, one could easily obtain the total number of photons detected by the charge coupled device (CCD), which is the integration of the luminescence spectrum ($3.55*10^4$) multipled by a factor of 2.0 (to account for the luminescence removed by the filter), to be N_2^{pl} ~ $2*3.55*10^4$. Based on the method used for estimatiing the quantum efficiency, which will be described later in Supplementray Note 13, the total number of photons emitted by the Si nanoparticle was deduced to be $N_1^{pl} = 2.34*10^{13}$ according to Eq. (3) (see Supplementary Note 13). Since the repetition rate of the femtosecond laser pulses is 76 MHz and the total number of photons emitted from the Si nanoparticle was detected within a time duration of t = 1.0 s (the exposure time of the CCD), the number of photons emitted from the Si nanoparticle after the excitation of a single pulse was calculated to be $n_1^{pl} = 2.34*10^{13}/76*10^6 = 3.08*10^5$. If we assumed a quantum efficiency of Q~3.5% for the Si nanoparticle, which is close to the value described laser in Supplementary Note 13, then the number of carriers generated in the Si nanoparticle by a single femtosecond laser pulse was estimated to be n_1^{abs} ~$3.08*10^5/0.035 = 1.03*10^7$. This number of injected carrers corresponds to a carrier density of ~$2.56*10^{21}$ cm^{-3} because volume of the Si nanoparticle (R ~ 90 nm) was estimated to be ~$2.75*10^{15}$ cm^3. From Figure S3c, we can estimate the refractive index change induced by injected carriers to be Δn ~ -0.32. Since the negative refractive index change is counteracted by the positive one induced by the thermo-optical effect described in Figure S3b, we could deduce the temperature of the Si nanoparticle (after the luminescence burst) to be ~1520 K.

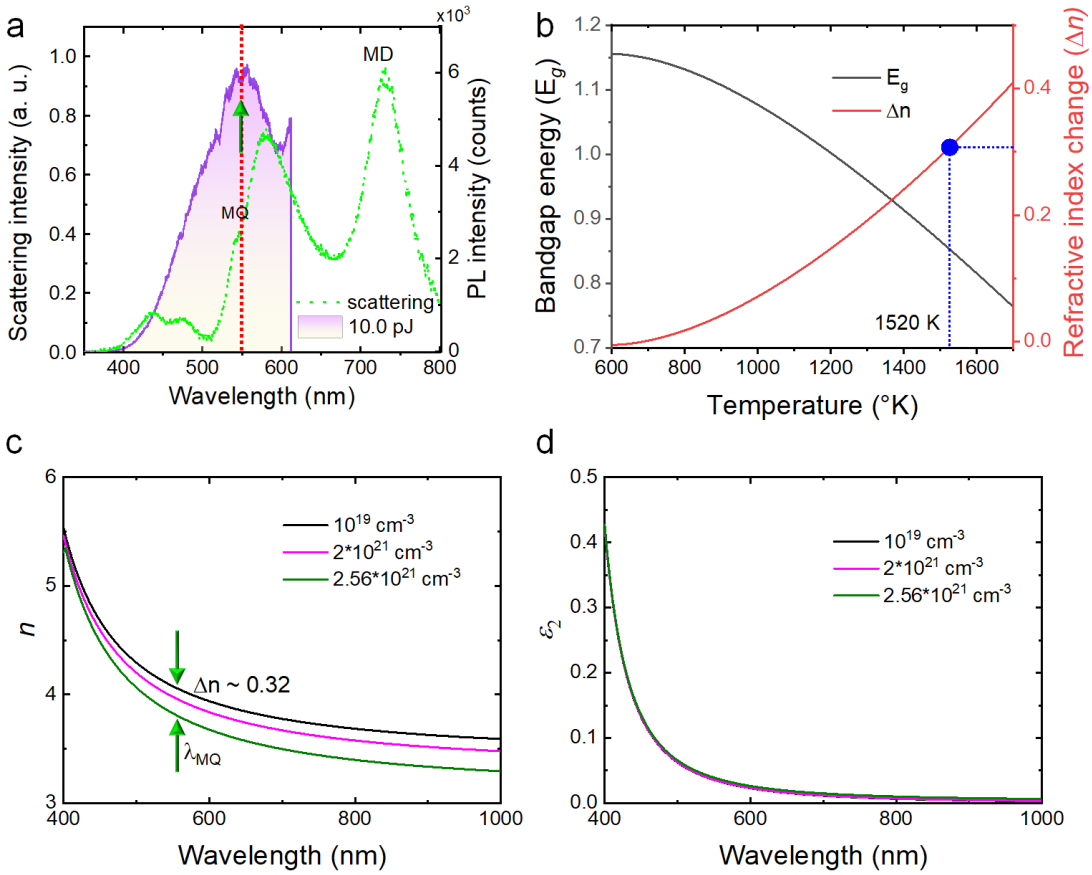

Figure S3 (a) Luminescence spectrum measured for a Si nanoparticle placed on a SiO_2 substrate at an excitation pulse energy of 10.0 pJ (reproduced from Figure 2a). Also shown is the scattering spectrum of the Si nanoparticle. (b) Dependence of the bandgap energy E_g and refractive index change Δn (real part) of Si on the temperature induced by the thermo-optical effect. (c) and (d) Refractive index change of Si (real and imagnary parts, n and κ) induced by injected carriers with different densities.

Supplementary Note 5: Characterization of damaged Si nanoparticles

It was found that the Si nanoparticles placed on the SiO_2 are easily damaged, probably due to the large threshold and the poor thermal conductivity of the SiO_2 substrate. In Figure S4a, we presented the scattering spectra measured for a damaged Si nanoparticle (before and after the luminescence burst). It can be seen that the distinct electric and magnetic dipoles in the Si nanoparticle disappear completely after the damage. A single scattering peak at a shorter wavelength of ~500 nm was observed. In Figure S4b, we show the scanning electron microscope (SEM) image of the Si nanoparticle after the damage, where a smaller Si nanoparticle with irregular shape was observed.

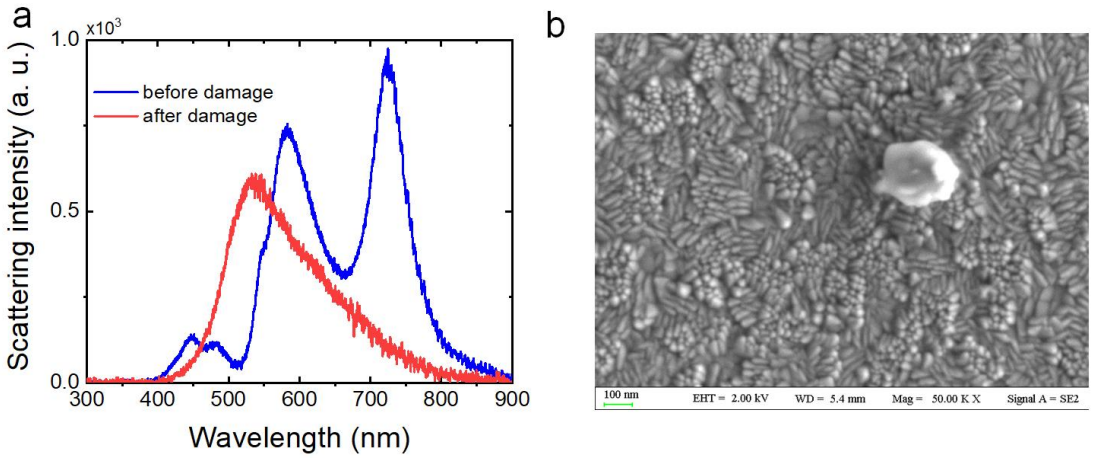

Figure S4 (a) Scattering spectra measured for a Si nanoparticle on the SiO_2 substrate before and after the demage. (b) SEM image of the Si nanoparticle after the damage.

Supplementary Note 6: Purcell factors and mode volumes calculated for Si nanoparticles on different substrates

Basically, the hot electron luminescence of a Si nanoparticle is determined by the Purcell factor which is governed by the enhancement of the electric field and the mode volume. We calculated the distributions of the Purcell factor on the cross section of a Si nanoparticle (with a diameter of 180 nm) on the SiO_2/Ag/SiO_2 substrate at two wavelengths of 580 and 810 nm, as shown in Figure S5. It can be seen that a Purcell factor as large as several hundred can be achieved at the contact point between the Si nanoparticle and the Ag film. It implies a significant enhancement of the electric field at the contact point due to the formation of mirror-image-induced magnetic dipole resonance.

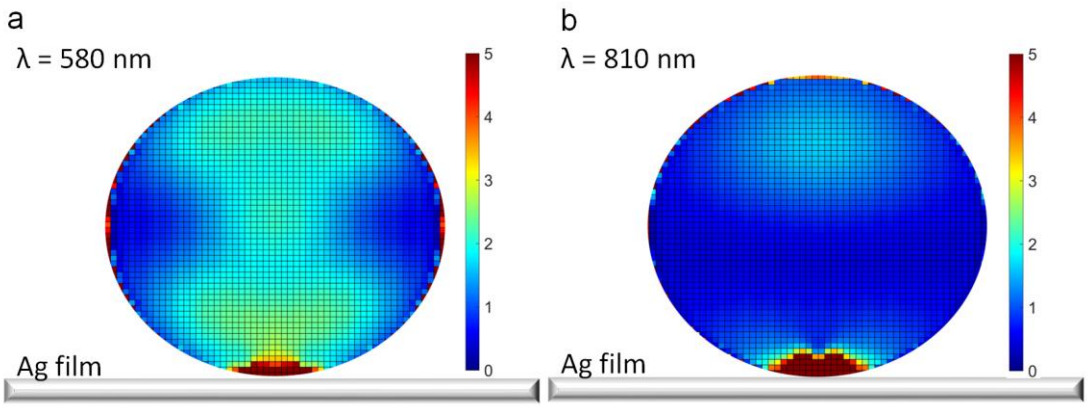

Figure S5 Distribution of the Purcell factor on the cross section of a Si nanoparticle (d = 180 nm) placed on a SnO_2/Ag/SiO_2 substrate calculated at the two optical resonances of the Si nanoparticle (λ = 580 and 810 nm). The meshes on the cross section of the Si nanoparticle represent the locations of the dipole sources used to extract the local Purcell factors. Here, the Ag film is only a sketch, not the screenshot in the numerical simulation.

Supplementary Note 7: Electric field enhancements in Si nanoparticles on different substrates

In Figure S6, we present the scattering spectra calculated for two Si nanoparticles with the same diameter of d = 200 nm placed on a SiO_2 and a SnO_2/Ag/SiO_2 substrate, respectively. Also shown are the integrations of $|E|^4$ and $|E|^6$ over the volume the Si nanoparticle (i.e., $\int|E(\lambda)|^4 dV]/V$ and $\int|E(\lambda)|^6 dV]/V$), which represent the 2PA and 3PA of the Si nanoparticle, respectively. It is remarkable that the 2PA and 3PA of the Si nanoparticle are enhanced by factors of ~3 and 35 when it is placed on the SnO_2/Ag/SiO_2 substrate.

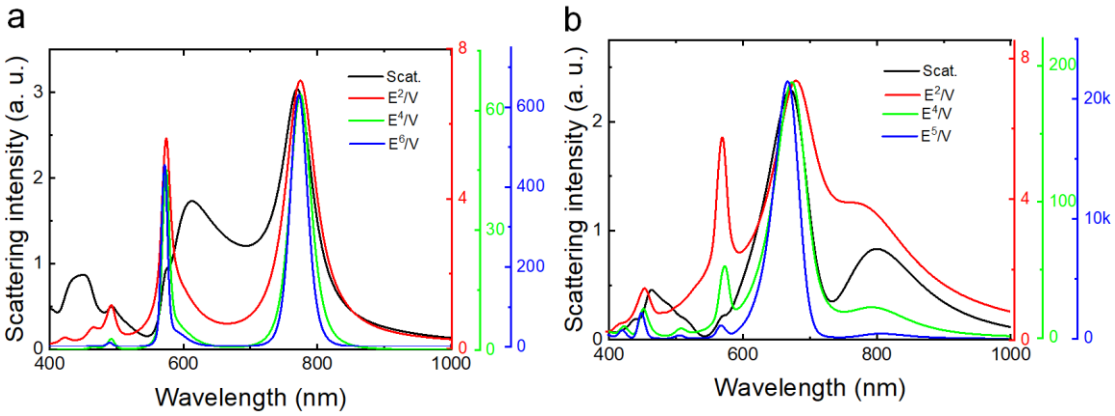

Figure. S6 Scattering spectra and the corresponding $\int|E(\lambda)|^4 dV]/V$ and $\int|E(\lambda)|^6 dV]/V$ spectra calculated for Si nanoparticles with d = 200 nm placed on a SiO_2 (a) and a SnO_2/Ag/SiO_2 (b) substrate.

Supplementary Note 8: Mode identification based on the multipole expansion method

In Figure S7a, we show the backward scattering spectrum (Total) calculated for a Si nanoparticle (d = 200 nm) placed on a SnO_2/Ag/SiO_2 substrate (normal incidence). Multipole expansion method is employed to extract the contributions of the electric and magnetic dipoles and quadrupoles (p_x, m_y, EQ, MQ). The electric dipole (p_x) is located at ~650 nm. In Figure S7b, we present the scattering spectra measured by using *p*- or *s* –polarized light as the excitation source (oblique incidence) and *p*- or *s*-polarized analyzer as the filter. The p_x mode can be revealed at ~660 nm by exciting the Si nanoparticle with *s*–polarized light and filtering the scattering light with a *s*-polarized analyzer (the blue curve). Similarly, the scattering peak appearing ~720 nm is attributed to the radiation of the m_z mode, which can be revealed by exciting the Si nanoparticle with *s*–polarized light and filtering the scattering light with a *p*-polarized analyzer (the pink curve).

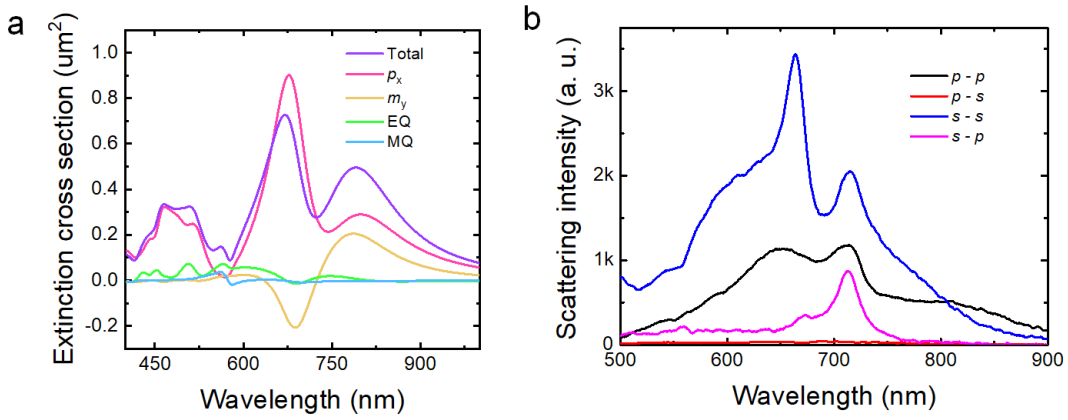

Figure. S7 (a) Backward scattering spectrum calculated for a Si nanoparticle (d = 200 nm) placed on a SnO_2/Ag/SiO_2 substrate. (b) Scattering spectra measured for a Si nanoparticle (d ~ 200 nm) placed a SnO_2/Ag/SiO_2 substrate. The Si nanoparticle is excited by using p- and s-polarized light and the scattering light is analyzed by using a p- or s-polarized analyzer.

Supplementary Note 9: Multiple measurements of the luminescence burst

As discussed in the main text, stable emission of white light can be ahieved in Si nanoparticles placed on the SnO_2/Ag/SiO_2 substrate. In order to examine the stability of the white light emission, we chose a Si nanoparticle and repeated the meausrement of luminescence burst for three times, as shown in Figure S8a–c. In Figure S8d–f, we plot the averaged luminescence intensity of the Si nanoparticle as a function of the excitation pulse energy at three wavelengths of λ = 500, 500, and 600 nm with error bars. It can be seen that the luminescence intensity remains nearly unchanged below the threshold. However, a fluctuation in the luminescence intensity is observed above the threhsold.

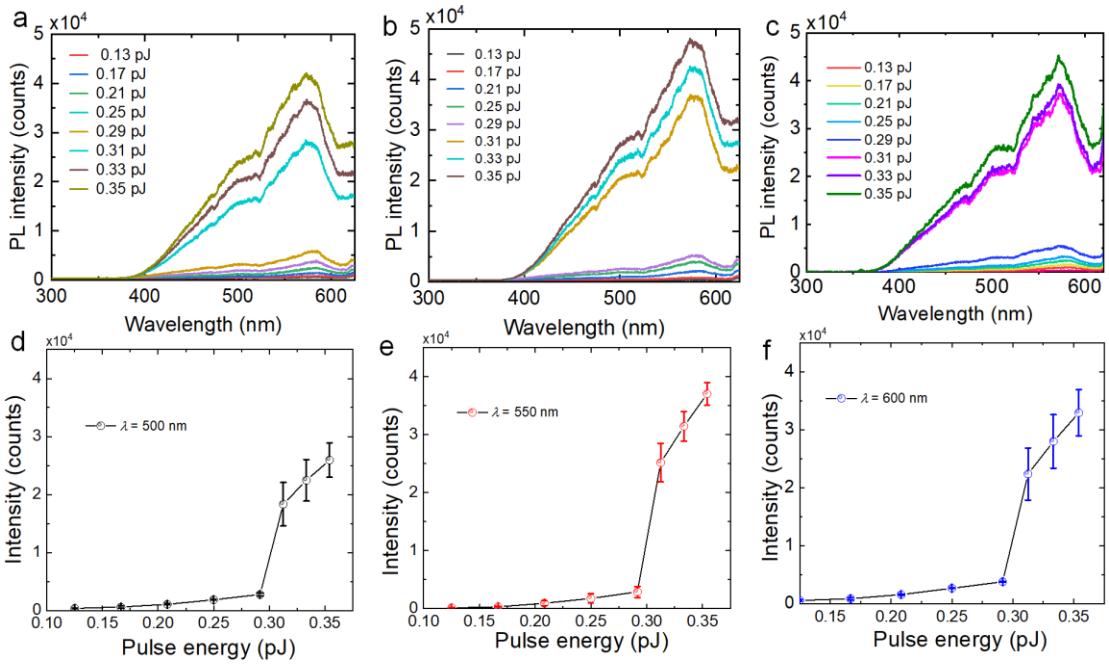

Figure S8 (a-c) Luminescence spectra of a Si nanoparticle on the SnO_2/Ag/SiO_2 substrate measured at

different rounds. (d-f) Dependence of the averaged luminescence intensity on the excitation pulse energy extracted for three different wavelengths.

Supplementary Note 10: Changes in optical scattering and morphology after the luminescence burst

It is desirable to know the changes in both the optical properties and the morphology of a Si nanoparticle after the luminesence burst because the Si nanoparticle suffers from a high-temperature "annealing" process. In Figure S9a, we show the forward scattering spectra measured for a Si nanoparticle on the $SnO_2/Ag/SiO_2$ substrate before and after the luminescence burst. One can find a small blue shift of the mirror-image-induced MD resonance and a slightly broadneing of its linewidth. We also examined the morphologies of the Si nanoprticle before and after the luminescence burst, as shown in Figire S9b,c. It was found that the dimension of the Si nanoparticle in the vertical direction is slightly inceased.

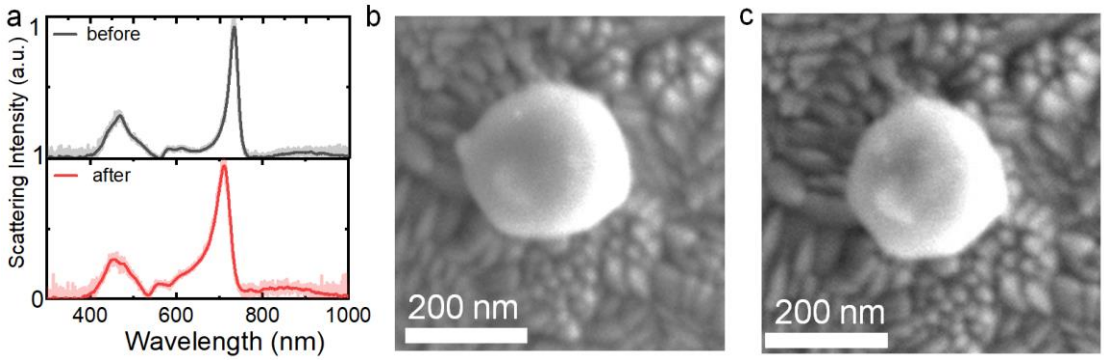

Figure. S9 (a) Forward scattering spectra measured for a Si nanoparticle before and after the luminescence burst. The SEM images of the Si nanoparticle before and after the luminescence burst are shown in (b) and (c), respectively.

Supplementary Note 11: Collection efficiency of the luminescence

We calculated the total collection efficiency of the emitted photons from a Si nanoparticle placed on the $SnO_2/Ag/SiO_2$ substrate by considering both the external quantum efficiency of the Si nanoparticle (i.e., including the linear absorption of the Si nanoparticle) and the collection efficiency of the 100× objective lens with a numerical aperture (NA) of ~1.40. First, the directional emission efficiency of an ED emitter at a certain wavelength was calculated by averaging the directional emission intensities obtained at different locations inside the Si nanoparticle. For each location, the averaged value for three orthogonal orientations of the ED emitter was derived. Then, the wavelength-dependent total collection efficiency was obtained by using Fourier transform of the time domain signal under the excitation of a Gaussian pulse. The $SnO_2/Ag/SiO_2$ substrate used to support the Si nanoparticle was also taken into account. Finally, the collection efficiency of the objective lens was calculated by evaluating the near- to far-field projection over a cone defined by the NA of the objective lens. In Figure S10, we show the collection efficiencies calculated for the Si nanoparticle at different wavelengths. The scattering spectrum of the Si nanoparticle is also provided for reference. It can be seen that an averaged collection efficiency of 0.52 is

obtained in the visible to near infrared spectral range (400–900 nm), which is larger by a factor of ~4.0 as compared with that for the Si nanoparticle supported by a SiO_2 substrate (see Ref. 23).

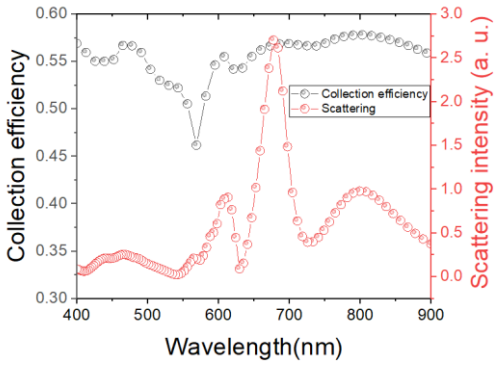

Figure. S10 Collection efficiencies calculated for a Si nanoparticle on the SnO_2/Ag/SiO_2 substrate at different wavelengths. Also shown is the scattering spectrum of the Si nanoparticle.

Supplementary Note 12: Excitation efficiencies for the modified p_x and m_z modes

We fixed the excitation wavelength at 720 nm and compared the excitation efficiencies at the p_x and m_z modes by choosing Si nanoparticles with different diameters of 185 and 205 nm. The backward scattering spectra measured for these two Si nanoparticles are shown in Figure S11a. It can be seen that the p_x and m_z modes of the two Si nanoparticles are located at ~720 nm. In Figure S11b, we show the excitations spectra measured for these two Si nanoparticles. For the Si nanoparticle whose resonant peak appearing at 720 nm, the strongest luminescence intensity is really achieved at the resonant wavelength. In comparison, the strongest luminescence intensity is not obtained at the resonant wavelength of the m_z mode. This behavior indicates that the excitation efficiency at the p_x mode is much larger than that at the m_z mode. In Figure S11c, we present the dependence of the luminescence intensity on the excitation pulse energy measured for the two Si nanoparticles. Burst of luminescence is observed for the Si nanoparticle excited at p_x mode. For the Si nanoparticle excited at the m_z mode, the damage of the Si nanoparticle occurs when the excitation pulse energy is larger than 2.8 pJ.

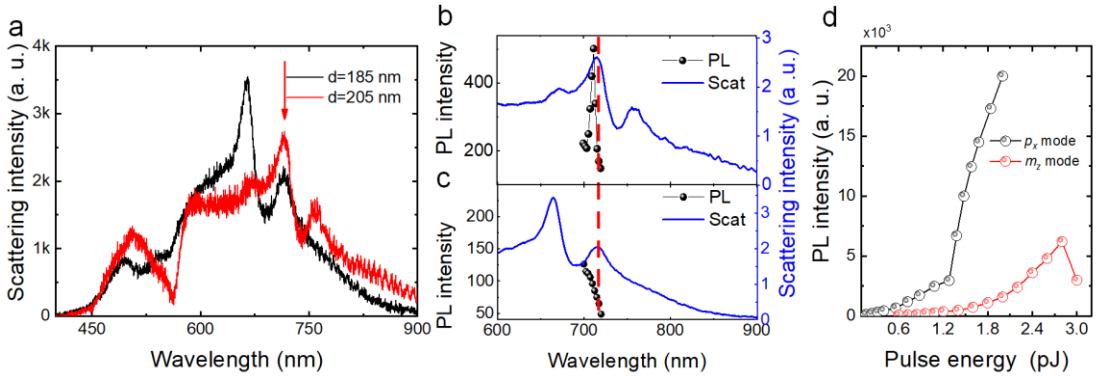

Figure S11 (a) Backward scattering spectra measured Si nanoparticles with d = 185 and d = 205 nm. (b) Excitation spectra measured for the two Si nanoparticles shown in (a). (c) Dependence of the luminescence intensity on the excitation pulse energy measured for the two Si nanoparticles shown in (a).

Supplementary Note 13: Estimation of quantum efficiency

The method used to estimate the quantum efficiency of the hot electron lumindescence from Si nanoparticles was the same as that described in our previous work (see Supplementary Note 3 in Ref. 23). Since the estimation of quantum efficiency relies on the detection of the reflected laser light, which is not available for the dichroic mirror and filter used for the optical parametric oscillator, which was used in the experiments shown in Figure 3, we chose to excite Si nanoparticles on the SnO_2/Ag/SiO_2 substrate with their optical resonances at longer wavelengths by using femtosecond laser pulses at ~720 nm. In Figure S12a,b, we show the optical pathes of the excitation laser light (λ_1 ~ 720 nm) and the generated hot electroc luminescence (λ_2 < 620 nm in Figure 2 and 640 nm < λ_2 < 670 nm in Figure 3) in the experimental setup used to simultaneously excite Si nanoparticles and to collect/detect the optical signals. The Si nanoparticle being characterized could be located on a SiO_2 substrate or on an SnO_2/Ag/SiO_2 substrate. In Figure S12a, it can be seen that the femtosecond laser light is reflected by a dichroic mirror and focused on the Si nanoparticle by the objective lens of the microscope. The reflected laser light from the Si nanoparticle on the substrate is attenuated by the combination of the dichroic mirror and a long-pass filter with an optical density of $OD \sim 2.3 \times 10^{-6}$. If we assume that the attenuation cofficient of the whole optical system (except the dichroic mirror + filter) is α, and the gain and quantum effiency of the charge coupled device (CCD) are g_{ex} and η_{ex} (~0.80 at 720 nm, see Figure S12c), then the total number of photons detected by the CCD, i.e., N_2^{ex}, can be expressd as follows:

$$N_1^{ex} * r * OD * \alpha * g_{ex} * \eta_{ex} = N_2^{ex}, \quad (1)$$

where N_1^{ex} represents the total number of photons irradiating on the Si nanoparticle and the substrate and r demotes the corresponding reflectivity (see Figure S12a).

If we compared the intensity of the reflected light from the substrate without and with the Si nanoparticle, a small reduction is observed, as shown in Figure S12d. This reduction is induced by the linear absorption and scattering of the excitation laser light by the Si nanoparticle. When we examined the dependence of the reflected light intensity on the excitation pulse energy (or excitation power), a linear relationship is observed at low excitation pulse energies, as shown in Figures 13d, 14d, and 15d. When the excitation pulse energy exceeds a critical value (or a threshold), a deviation from the linear relationship occurs, implying that the nonlinear absorption (e.g., two-photon-induced absorption) of the Si nanoparticle becomes effective (see also Figures 13d, 14d, and 15d) Apparently, the photons absorbed by the Si nanoparticle via two-photon-induced absorption can be deduced from the reduction in the reflected light intensity (or the deviation of the reflected light intensity from the linear relationship), as indicated by the arrows in Figures 13d, 14d, and 15d. Therefore, the number of photons absorbed by the Si nanoparticles (N_1^{abs}) due to nonlinear processes can

be deduced by the number of reduced photons observed in the reflected light (N_2^{abs}) by the following relationship:

$$N_1^{abs} * r * OD * \alpha * g_{ex} * \eta_{ex} = N_2^{abs}. \quad (2)$$

Referring to Figure 12b, we can obtain the similar relationship between the number of detected photons (N_2^{pl}) in the luminescence and the number of emitted photons from the Si nanoparticle (N_1^{pl}), which is given in the following:

$$N_1^{pl} * \beta * \alpha * g_{pl} * \eta_{pl} = N_2^{pl}. \quad (3)$$

Here, the collection efficiency of the objective lens (β) is taken into account. The value β depends strongly on the substrate used to support the Si nanoparticle. For Si nanoparticles located on the $SnO_2/Ag/SiO_2$ substrate, the average collection efficiency in the visible to near infrared spectral range was found to be $\beta \sim 0.52$ (see Supplementary Note 11).

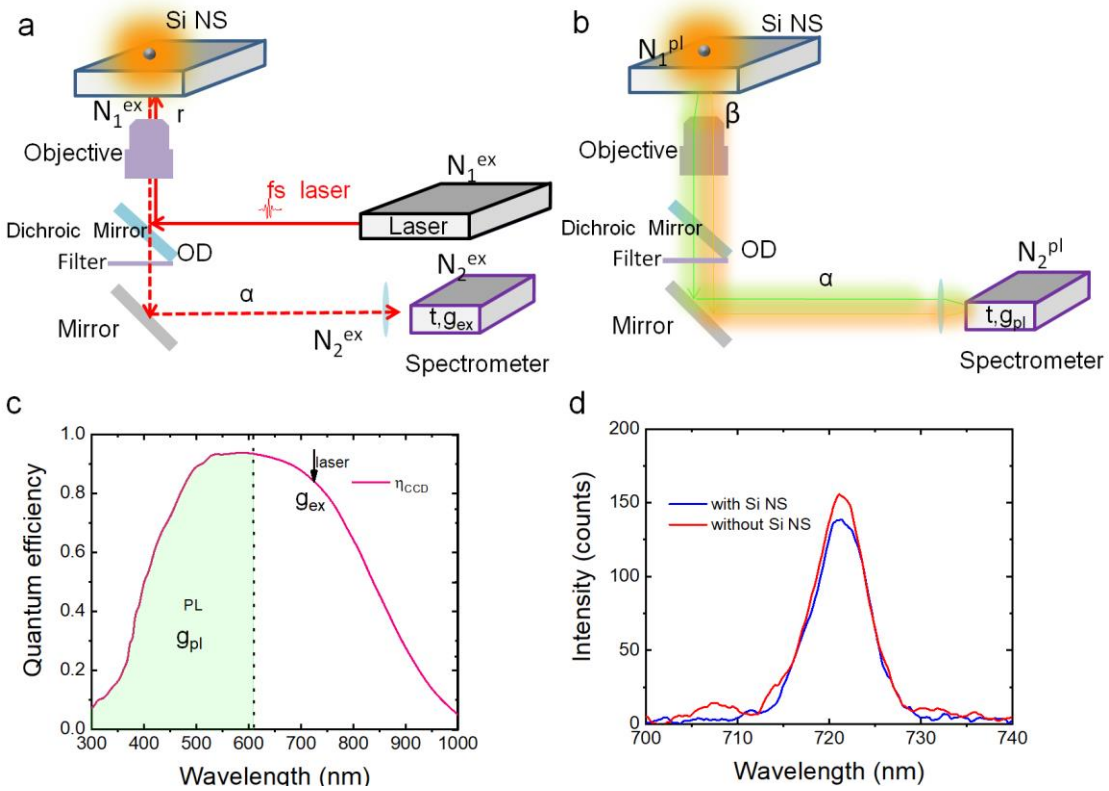

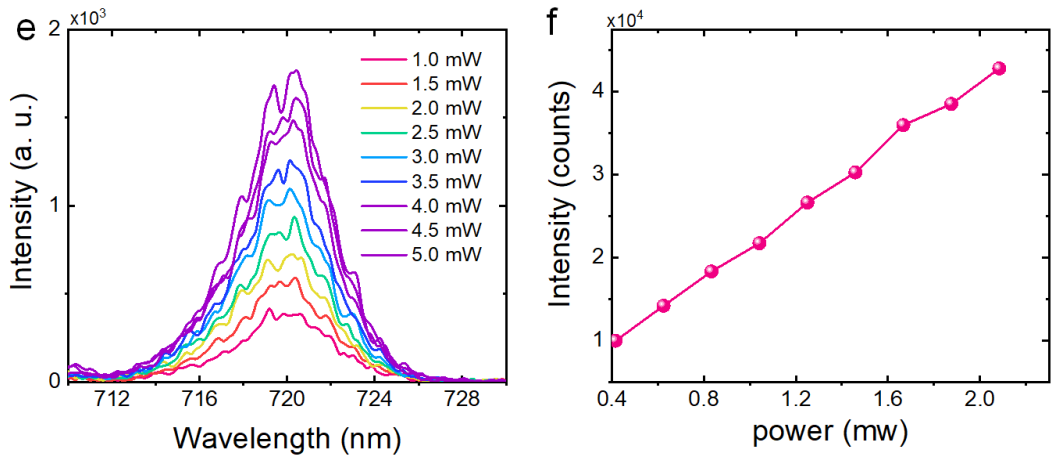

Figure. S12 Schematics showing the optical paths of the excitation laser light (a) and the luminescence emitted from a Si nanoparticle (b) in the experiment setup used to estimate the quantum efficiency of the Si nanoparticle. (c) Wavelength dependence of the quantum efficiency of the CCD. (d) Reflection spectra of the laser light without and with the Si nanoparticle. (e) Reflection spectra of the laser light with different powers. (f) Dependence of the integrated intensity of the reflected laser light on the laser power.

With the information on the number of photons absorbed by the Si nanoparticle (N_1^{abs}) and that emitted from the Si nanoparticle (N_1^{pl}), one can readily derive the quantum efficiency of the hot electron luminescence, which is expressed as follows:

$$Q = N_1^{pl}/N_1^{abs} = N_2^{pl} * r * OD * \eta_{ex}/(N_2^{abs} * \beta * \eta_{pl}). \quad (4)$$

The quantum efficiency would be $2Q$ or $3Q$ if a two- or three-photon-induced absorption is involved in the generation of carriers. From Eq. (4), it is remarkable that the quantum efficiency Q is independent on the attenuation coefficient of the optical system (α) because both the reflected laser light and the generated luminescence suffer the same attenuation before reaching the detector. Hence, the attenuation coefficient is cancelled out in the final expression of the quantum efficiency. However, the information of the attenuation coefficient is necessary if we want to derive the total number of photons absorbed by the Si nanoparticle or the total number of photons emitted from the Si nanoparticle (see Eq. (2) and Eq. (3)). Basically, the value of α is determined mainly by the optical coupling between the microscope and the spectrometer, especially the slit width of the spectrometer. In this work, the slit width was intentionally reduced in order to avoid the saturation of the CCD, which might occur in the burst of luminescence.

In order to accurately derive the attenuation coefficient, we measured the reflection spectra of the laser light (720 nm) with different powers, as shown in Figure 12e. In Figure 12f, we plot the integrated intensities of the reflected laser light as a function of laser power and observed a linear relationship. The exposure time and gain of the CCD were chosen to be t = 1.0 s and g_{ex} = 100. In this experiment, we observed a laser power of ~0.4 mW after the objective lens if we delivered a laser light of 1.0 mW into the microscope (see Figure 12a). Then, the laser light reflected by the $SnO_2/Ag/SiO_2$ substrate (with a reflectivity of $r \sim 0.80$ at

720 nm) entered into the microscope again through the objective lens, passing though the dichroic mirror and filter, and finally reaching the CCD. Apparently, the number of photons in the laser light before the reflection (N_1^{ex}) and that detected by the CCD (N_2^{ex}) can be related by using Eq. (1). In this case, we have N_1^{ex} = 0.4 mJ/1.72 eV = 3.63 × 10^{15}, N_2^{ex} = 9.9 × 10^3 (see Figure 12f), r = 0.80, OD = 2.3 × 10^{-6}, g_{ex} = 100, η_{ex} = 0.80. With all these data, the attenuation coefficient of the optical system was derived to be $\alpha \sim 4.6 \times 10^{-8}$. It will be used later to obtain the total number of photons absorbed by the Si nanoparticle or the total number of photons emitted from the Si nanoparticle (see Eq. (2) and Eq. (3)).

In our experiments, we have measured several Si nanoparticles and estimated the quantum efficiencies of their luminescence, as shown in the following. The parameters used in the estimation of quantum efficiency are: r = 0.80, β = 0.52, OD = 2.3 × 10^{-6}, α = 4.6 × 10^{-8}, t = 1.0 s, g = 100, η_{ex} = 0.80, η_{pl} = 0.55.

Example No. 1: This is a Si nanoparticle located on the SnO_2/Ag/SiO_2 substrate whose scattering spectrum is shown in Figure S13a. The excitation wavelength was chosen to be $\lambda \sim$ 720 nm so that the mirror-image-induced MD resonance of the Si nanoparticle (~710 nm) was almost resonantly excited. The evolution of the luminescence spectrum with increasing excitation pulse energy is shown in Figure S13b while the corresponding reflection spectra of the excitation laser light at different pulse energies are presented in Figure S13c. It can be seen that the luminescence burst appears at excitation pulse energy of ~1.0 pJ. The dependences of the integrated intensities of the luminescence and the reflected laser light on the excitation pulse energy are presented on Figure S13d. Based on Figure S13d, the number of photons absorbed by the Si nanoparticle (N_2^{abs}) and that emitted from the Si nanoparticle (N_2^{pl}), which are two quantities necessary for estimating the quantum efficiency (see Eq. (4)), can be easily obtained. In this case, we have N_2^{abs} = 2.77 × 10^3 and N_2^{pl} = 2.66 × 10^6 at 0.88 pJ (below the threshold) and N_2^{abs} = 2.97 × 10^3 and N_2^{pl} = 1.96 × 10^7 at 1.0 pJ (above the threshold). As a reasonable approximation, the value of N_2^{pl} has been doubled (×2) in order to account for the luminescence removed by the filter. The quantum efficiencies for the Si nanoparticle are derived to be $Q \sim$ 0.5% and $Q \sim$ 3.0% based on Eq. (4). If we consider two-photon-induced absorption as the dominant process for generating carriers, then the quantum efficiencies of the luminescence would be $Q \sim$ 1.0% and Q ~6.0% below and above the threshold, respectively.

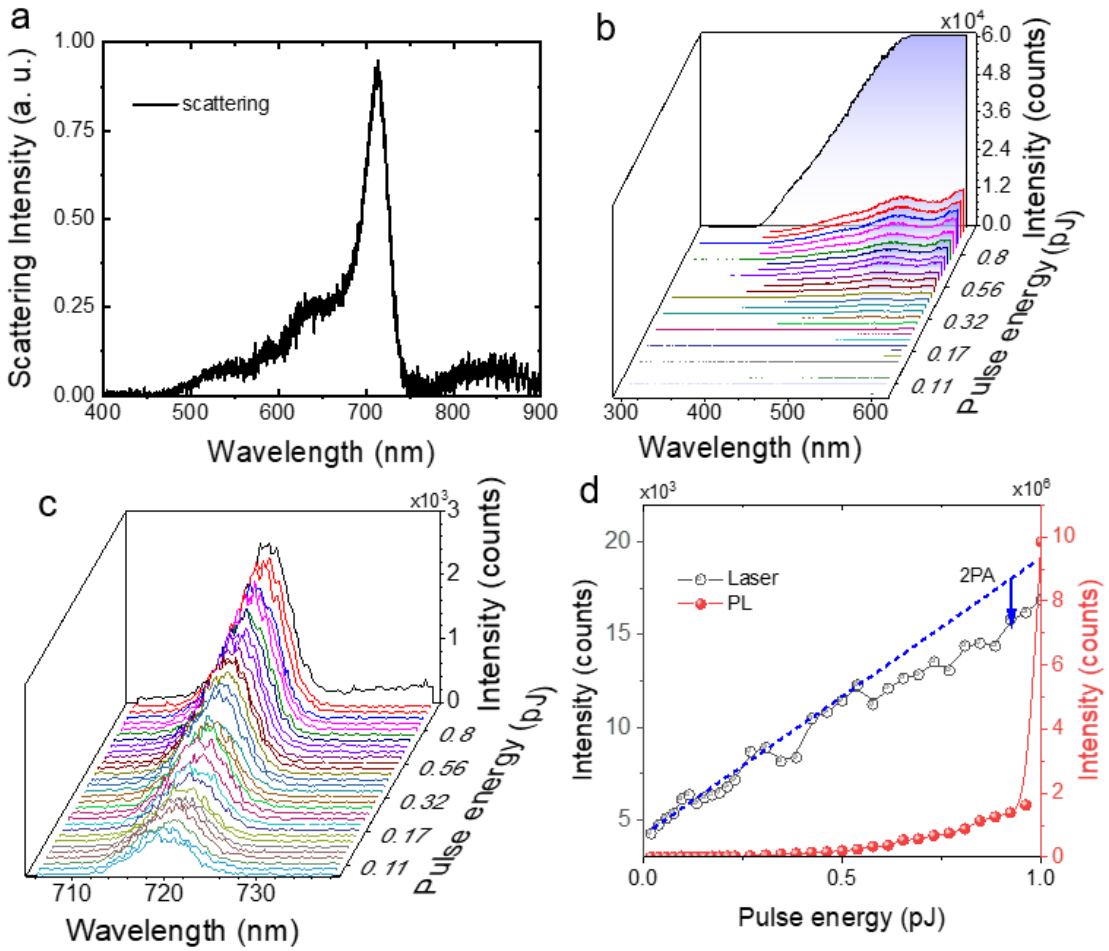

Figure S13 (a) Scattering spectrum of a Si nanoparticle (No. 1) located on the SnO_2/Ag/SiO_2 substrate. (b) Evolution of the luminescence spectrum with increasing excitation pulse energy. (c) Evolution of the reflection spectrum of the excitation laser light with increasing excitation pulse energy. (d) Dependences of the integrated intensities of the luminescence and the reflected laser light on the excitation pulse energy.

Example No. 2: This is a Si nanoparticle located on the SnO_2/Ag/SiO_2 substrate whose scattering spectrum is shown in Figure S14a. The excitation wavelength was chosen to be $\lambda \sim$ 720 nm which was close to the mirror-image-induced MD resonance of the Si nanoparticle (~700 nm). The evolution of the luminescence spectrum with increasing excitation pulse energy is shown in Figure S13b while the corresponding reflection spectra of the excitation laser light at different pulse energies are presented in Figure S13c. It can be seen that the luminescence burst appears at excitation pulse energy smaller than 1.0 pJ. The dependences of the integrated intensities of the luminescence and the reflected laser light on the excitation pulse energy are presented on Figure S13d. Based on Figure S13d, the number of photons absorbed by the Si nanoparticle (N_2^{abs}) and that emitted from the Si nanoparticle (N_2^{pl}), which are two quantities necessary for estimating the quantum efficiency (see Eq. (4)), can be easily obtained. In this case, we have $N_2^{abs} = 1.30 \times 10^5$ and $N_2^{pl} = 2.60 \times 10^7$ at 0.8 pJ (below the threshold) and $N_2^{abs} = 1.64 \times 10^4$ and $N_2^{pl} = 3.76 \times 10^7$ at 1.0 pJ (above the threshold). As a

reasonable approximation, the value of N_2^{pl} has been doubled (×2) in order to account for the luminescence removed by the filter. The quantum efficiencies for the Si nanoparticle are derived to be Q ~ 0.2% and Q ~1.4% based on Eq. (4). If we consider two-photon-induced absorption as the dominant process for generating the carriers, then the quantum efficiencies of the luminescence would be Q ~ 0.4% and Q ~2.8% below and above the threshold, respectively.

.

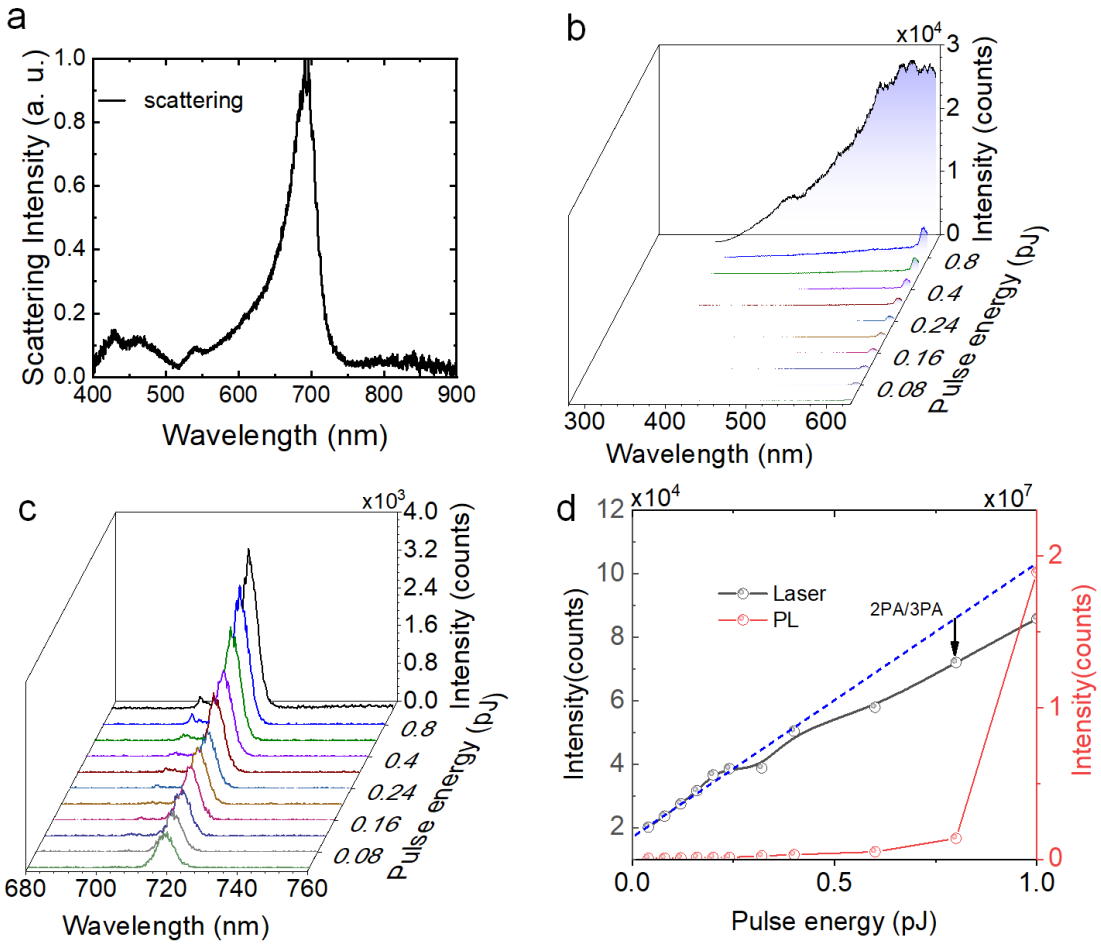

Figure S14 (a) Scattering spectrum of a Si nanoparticle (No. 2) located on the SnO_2/Ag/SiO_2 substrate. (b) Evolution of the luminescence with increasing excitation pulse energy. (c) Evolution of the reflection spectrum of the excitation laser light with increasing excitation pulse energy. (d) Dependences of the integrated intensities of the luminescence and the reflected laser light on the excitation pulse energy.

Example No. 3 This a Si nanoparticle located on the SnO_2/Ag/SiO_2 substrate whose scattering spectrum is shown in Figure S15a. The excitation wavelength was chosen to be λ ~ 720 nm so that the mirror-image-induced MD resonance of the Si nanoparticle (~720 nm) was resonantly excited. The evolution of the luminescence spectrum with increasing excitation pulse energy is shown in Figure S15b while the corresponding reflection spectra of the excitation laser light at different pulse energies are presented in Figure S15c. It can be seen that the luminescence burst appears at excitation pulse energy of ~0.52 pJ. The dependences of the integrated intensities of the

luminescence and the reflected laser light on the excitation pulse energy are presented on Figure S15d. Based on Figure S15d, the number of photons absorbed by the Si nanoparticle (N_2^{abs}) and that emitted from the Si nanoparticle (N_2^{pl}), which are two quantities necessary for estimating the quantum efficiency (see Eq. (4)), can be easily obtained. In this case, we have $N_2^{abs} = 3.07 \times 10^2$ and $N_2^{pl} = 8.60 \times 10^5$ at 0.41 pJ (below the threshold) and $N_2^{abs} = 4.05 \times 10^3$ and $N_2^{pl} = 3.02 \times 10^7$ at 0.52 pJ (above the threshold). As a reasonable approximation, the value of N_2^{pl} has been doubled (×2) in order to account for the luminescence removed by the filter. The quantum efficiencies for the Si nanoparticle are derived to be $Q \sim 1.7\%$ and $Q \sim 4.3\%$ based on Eq. (4). If we consider two-photon-induced absorption as the dominant process for generating the carriers, then the quantum efficiencies of the luminescence would be $Q \sim 3.4\%$ and $Q \sim 8.6\%$ below and above the threshold, respectively.

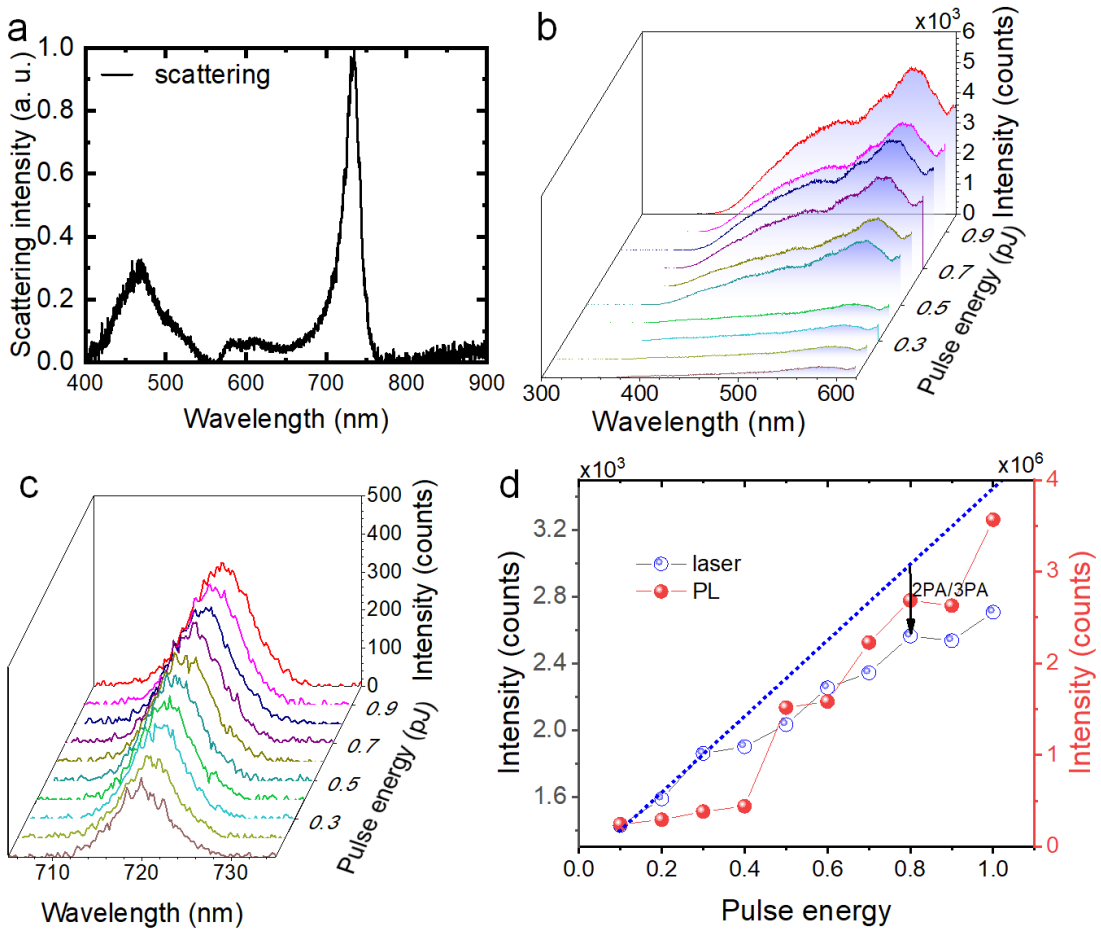

Figure S15 (a) Scattering spectrum of a Si nanoparticle (No. 3) located on the $SnO_2/Ag/SiO_2$. (b) Evolution of the luminescence with increasing excitation pulse energy. (c) Evolution of Evolution of the reflection spectrum of the excitation laser light with increasing excitation pulse energy. (d) Dependences of the integrated intensities of the luminescence and the reflected laser light on the excitation pulse energy.

Supplementary Note 14: Estimation of the thermal radiation energy of a Si nanoparticle

Since the melting point of Si is 1410°C, we considered the radiation a blackbody with a diameter of ~200 nm, which is the up limit of the thermal radiation energy of a Si nanoparticle with a diameter of 200 nm. We first calculated the radiation spectrum of the blackbody at a temperature of 1673°K (1400°C) by using the formula given in Eq. (5), as shown in Figure S16.

$$I(\lambda, T) = \frac{2hc^2}{\lambda} \frac{1}{e^{\frac{hc}{\lambda kT}} - 1}. \quad (5)$$

Here, h is the Planck constant, c is the speed of light in vacuum, k is the Boltzmann constant, λ is the wavelength of the electromagnetic radiation, and T is the absolute temperature of the blackbody. The dimension of I is $W \cdot sr^{-1} \cdot m^{-2} \cdot m^{-1}$. Owing to the existence of Mie resonances in the Si nanoparticle which modify the absorption efficiencies, the radiation intensity at the magnetic dipole (MD) resonance of the Si nanoparticle is greatly enhanced based on the Kirchhoff's law.[1] Here, we employed the Mie theory to calculate the absorption efficiency of the Si nanoparticle (d = 200 nm). As a result, the radiation spectrum of the Si nanoparticle is modified as compared with that of the blackbody given in Eq. (5), as shown in Figure S16. The total energy radiated by the Si nanoparticle in the visible to near infrared spectral range (300–900 nm) within a time period of t = 1.0 s was calculated to be $Q = 9.1 \times 10^{-9}$ J.

Now we used the Si nanoparticle shown in Figure S15 as an example to estimate the total energy of the photons emitted from the Si nanoparticle. In the estimation of the quantum efficiency described above (see Supplementary Note 13), we have extracted the attenuation coefficient of the measurement optical system, which was found to be $\alpha = 4.6 \times 10^{-8}$. Based on Eq. (3), the total number of photons in the luminescence can be deduced to be $N_l^{pl} \sim 3.95 \times 10^{13}$. If we used the photon energy at 610 nm, which is E_p = 2.0 eV or 3.2×10^{-19} J, as the averaged photon energy for the luminescence, the total energy of the luminescence was estimated to be $Q_{pl} = N_l^{pl} E_p \sim 1.26 \times 10^{-6}$ J. This value is more than two orders of magnitude larger than the blackbody radiation energy of the Si nanoparticle ($Q = 9.1 \times 10^{-9}$), implying that the emission from the Si nanoparticle is dominated by hot electron luminescence.

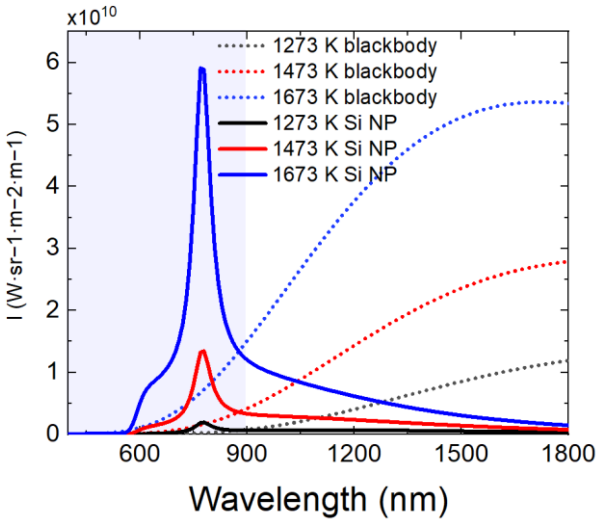

Figure S16 Radiation spectra calculated for a blackbody (dashed curves) and a Si nanoparticle (NP) (*d*

= 200 nm) (solid curves) at different temperatures. In each case, the radiation energy in the visible to near infrared spectral range (300–900 nm) can be derived from the area beneath the spectrum in this region.

Supplementary Note 15: Dependence of the luminescence intensity on the excitation pulse energy

By measuring the luminescence spectra of a Si nanoparticle excited at different powers (or pulse energies), which are shown in Figure 17a, we could find out the dependence of the luminescence intensity on the laser power below and above the threshold. The slopes extracted from the relationship between the luminescence intensity and the laser power plotted in a logarithmic coordinate at different wavelengths (or different energies of emitted photons) are presented Figure S17b. It is noticed that a slope of ~3.0 is observed in the wavelength range of 450–600 nm. This behavior is completely different from that observed for blackbody radiation, in which the slope is proportional to the energy of emitted photons. Here, the emission from Si nanoparticles arises from the interband transition of hot electrons assisted by optical resonances (see Figure 1a), which is clearly distinct from the intraband transition of hot electrons observed in plasmonic hot spots (see Ref. 28) or GaAs nanoparticles (see Ref. 29).

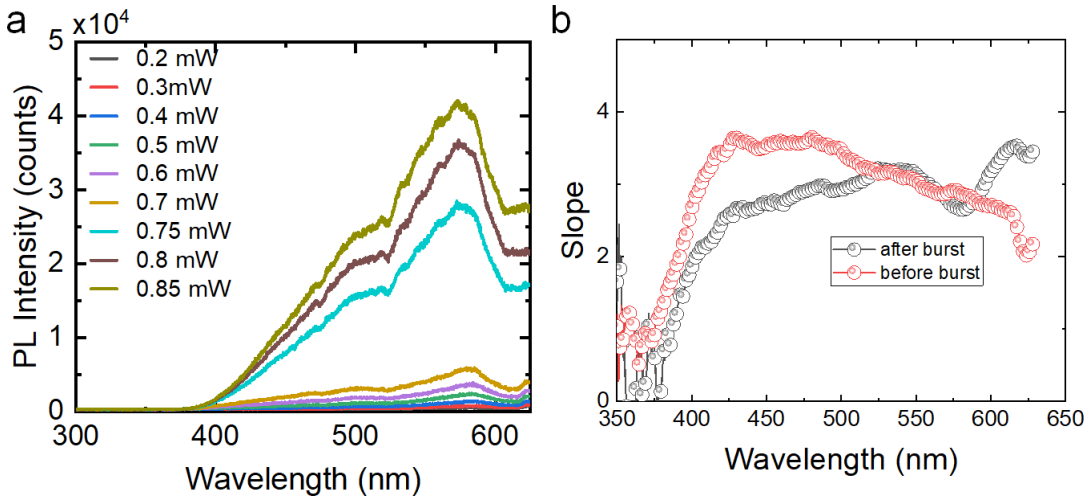

Figure S17 (a) Luminescence spectra measured for a Si nanoparticle excited at different powers. (b) Slopes extracted from the dependence of the luminescence intensity on the laser power plotted in a logarithmic coordinate at different wavelengths.

Supplementary Note 16: Luminescence lifetime measured at long wavelengths

In Figure 3, we show the luminescence of a Si nanoparticle placed on the SnO_2/Ag/SiO_2 substrate. In this case, an optical parametric oscillator (OPO) was employed to excite resonantly the mirror-image-induced MD of the Si nanoparticle. It is noticed that the luminescence is composed of an up- and a down-converted part. In our lab, the luminescence

lifetime was evaluated by using a TCSPC (time correlated single photon counting) system operating at a repetition rate of 3.8 MHz. Therefore, a pulse picker is necessary to reduce the repetition rate of the femtosecond laser pulses from 76 to 3.8 MHz. Owing to the low output of the OPO system, it cannot be used to measure the luminescence lifetime. In order to examine the luminescence lifetime at long wavelengths (in the down-converted part of the luminescence), we excited a Si nanoparticle by using the femtosecond laser oscillator operating at ~720 nm (with a repetition rate of ~3.8 MHz). The luminescence spectrum was measured by using a long-pass filter, as shown in Figure S18. The multiple peaks observed in the spectrum originate from the unknown interference effect in the optical system. It is noticed that the luminescence intensity decreases rapidly with increasing wavelength, which can be easily understood from the interband transition of electrons schematically shown in Figure 1a. The long-wavelength photons originate mainly from the indirect transition of hot electrons which needs the assistance of phonons. For this reason, it took a much longer time to obtain the luminescence decay at a long wavelength of ~780 nm, as shown in Figure S18b. The lifetime extracted from the exponential fitting of luminescence decay was found to be ~20 ps, quite similar to that observed at short wavelengths (see Figure 2d). The weak luminescence and short lifetime at long wavelengths further confirm that the emission from Si nanoparticles is dominated by hot electron luminescence with negligible thermal radiation.

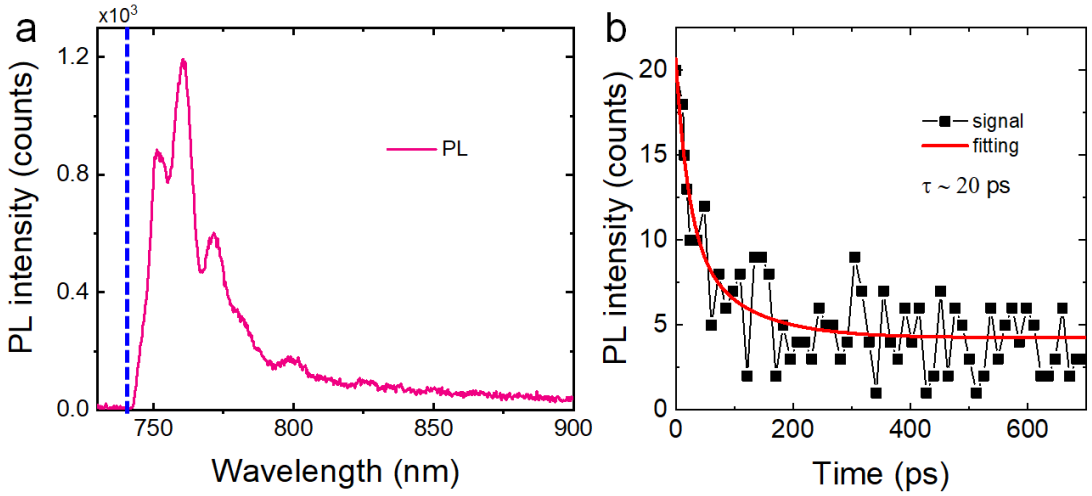

Figure S18 (a) Luminescence spectrum measured for a Si nanoparticle placed on the SnO_2/Ag/SiO_2 substrate by using a long-pass filter. (b) Luminescence decay measured for the Si nanoparticle at a wavelength of ~780 nm.

Supplementary Note 17: Analysis of the surface lattice resonator

In Figure S19, we present the transmission spectra calculated for the regular arrays of Si nanopillars (d = 240 nm) with a fixed period in y direction (l_y = 300 nm) and a varied period in the x direction (l_x). It can be seen that the transmission valley is redshifted when the period in the x direction is increased. For l_x ~ 400 nm, the transmission valley appears at ~720 nm. In order to reduce the nonradiative recombination centers, an oxidation process was employed to introduce a 50-nm-thick SiO_2 on the surfaces of Si nanopillars. In addition, the surface lattice

resonance at ~720 nm was achieved by filling the array of Si nanoparticles with $SiNO_x$ whose refractive index is ~1.7. In Figure S19b,c, we compare the electric field distribution on the *xz* plane calculated for a Si nanopillar in the regular array and a single Si nanopillar only, which are excited at 720 nm. It is noticed that electric field enhancement factor for the Si nanopillar in the regular array (~8.0) is much larger than that for the single Si nanopillar only (~1.0).

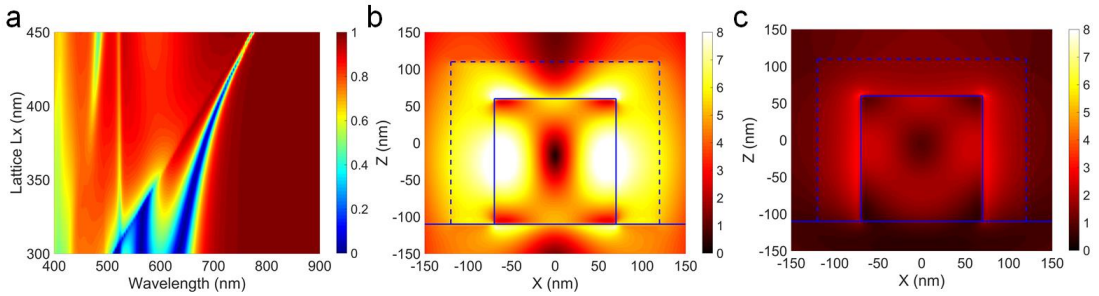

Figure S19 (a) Transmission spectra calculated for regular arrays of Si nanoparticles with a fixed period in the y direction (l_y = 300 nm) and a varied period in the x direction (l_x). (b) Electric field distribution on the xz plane calculated at 720 nm for a single Si nanopillar in the regular array with l_x = 400 nm and l_y = 300 nm. (c) Electric field distribution on the xz plane calculated at 720 nm for a single Si nanopillar only. In (b) and (c), the region is enclosed by solid lines is Si while the region between the solid and dashed lines is SiO_2.

Supplementary Note 18: Transmission spectrum of the surface lattice resonator

In Figure S20, we show the transmission spectra measured for the regular array of Si nanopillars without the $SiNO_x$ capping layer. In this case, we can see the redshift of the Mie resonances with increasing period. No surface lattice resonance is observed because the asymmetric refractive indices of air and substrate above and below the array of Si nanopillars.

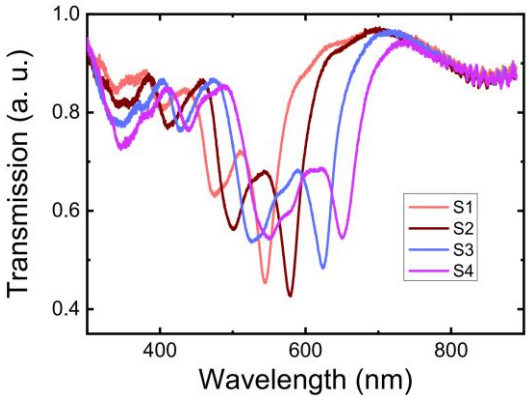

Figure S20 Transmission spectra measured for regular arrays of Si nanopillars with different lattice constants without the $SiNO_x$ capping layer.

reference

1: Bohren, C. F., & Huffman, D. R. (2008). *Absorption and scattering of light by small particles*. John Wiley & Sons.